On the structure and chemical bonding of Si_6^{2-} and Si_6^{2-} in $NaSi_6^-$ upon Na^+ coordination

Dmitry Yu. Zubarev, Anastassia N. Alexandrova,[a] and Alexander I. Boldyrev[b]
Department of Chemistry and Biochemistry, Utah State University, Logan, Utah 84322-0300

Li-Feng Cui, Xi Li,[c] and Lai-Sheng Wang[d]
Department of Physics, Washington State University, Richland, Washington 99354
and Chemical Sciences Division, Pacific Northwest National Laboratory, Richland, Washington 99352

(Received 12 January 2006; accepted 24 January 2006; published online 23 March 2006)

Photoelectron spectroscopy was combined with *ab initio* calculations to elucidate the structure and bonding in Si_6^{2-} and $NaSi_6^-$. Well-resolved electronic transitions were observed in the photoelectron spectra of Si_6^- and $NaSi_6^-$ at three photon energies (355, 266, and 193 nm). The spectra of $NaSi_6^-$ were observed to be similar to those of Si_6^- except that the electron binding energies of the former are lower, suggesting that the Si_6 motif in $NaSi_6^-$ is structurally and electronically similar to that in Si_6^-. The electron affinities of Si_6 and $NaSi_6$ were measured fairly accurately to be 2.23 ± 0.03 eV and 1.80 ± 0.05 eV, respectively. Global minimum structure searches for Si_6^{2-} and $NaSi_6^-$ were performed using gradient embedded genetic algorithm followed by B3LYP, MP2, and CCSD(T) calculations. Vertical electron detachment energies were calculated for the lowest Si_6^- and $NaSi_6^-$ structures at the CCSD(T)/6-311+G(2*df*), ROVGF/6-311+G(2*df*), UOVGF/6-311+G(2*d*), and time-dependent B3LYP/6-311+G(2*df*) levels of theory. Experimental vertical detachment energies were used to verify the global minimum structure for $NaSi_6^-$. Though the octahedral Si_6^{2-}, analogous to the closo form of borane $B_6H_6^{2-}$, is the most stable form for the bare hexasilicon dianion, it is not the kernel for the $NaSi_6^-$ global minimum. The most stable isomer of $NaSi_6^-$ is based on a Si_6^{2-} motif, which is distorted into C_{2v} symmetry similar to the ground state structure of Si_6^-. The octahedral Si_6^{2-} coordinated by a Na^+ is a low-lying isomer and was also observed experimentally. The chemical bonding in Si_6^{2-} and $NaSi_6^-$ was understood using natural bond orbital, molecular orbital, and electron localization function analyses. © *2006 American Institute of Physics*.
[DOI: 10.1063/1.2177254]

I. INTRODUCTION

Despite significant research efforts of many research groups, there is still no consistent theory of chemical bonding to describe silicon clusters, which are important both in chemistry as potential material building blocks and in nanoscience relevant to device design in the future. Doubly charged Si_x^{2-} clusters offer a unique opportunity to use the isolobal analogy between a HB unit and a Si atom to allow the application of the chemical bonding models developed for deltahedral boranes $(BH)_x^{2-}$.[1–3] The isolobal analogy between HB and Si would suggest a series of stable deltahedral Si_x^{2-} clusters analogous to the deltahedral $B_xH_x^{2-}$. However, this straightforward approach does not appear to work, because even though Si_5^{2-} is stable enough to be obtained and characterized in the solid state,[4] $B_5H_5^{2-}$ has not been synthesized.[1–3] On the other hand, Si_6^{2-} has not been synthesized yet, but $B_6H_6^{2-}$ is well known for its stability.[1–3] $B_{12}H_{12}^{2-}$, the most famous borane, is icosohedral in its most stable form, but the corresponding Si_{12}^{2-} cage is not the global minimum, albeit it is a higher-lying isomer. According to our preliminary results, the global minimum of Si_{12}^{2-} has a lower symmetry structure. Thus we need to develop a chemical bonding model capable of explaining why valence isoelectronic systems have different structures. Such chemical models will be the first step towards a comprehensive chemical bonding model for understanding the structure of silicon clusters.

The Si_6^{2-} cluster is the first system, which can be expected to have a highly symmetric octahedral structure, similar to the closo-borane $B_6H_6^{2-}$. However, a previous attempt to characterize the aromaticity of the octahedral Si_6^{2-} led to the conclusion that it is antiaromatic[5] and thus totally different from the corresponding aromatic $B_6H_6^{2-}$ closo borane. The difference was explained to be due to the mixing of the terminal hydrogen orbitals with the symmetry adapted skeletal molecular orbitals (MOs) of $B_6H_6^{2-}$, which lowers their energies relative to the corresponding lone pair-dominated Si_6^{2-} MOs, where such mixing is not possible.[5]

The hexasilicon cluster (neutral or with a negative charge) has been studied in numerous works with different theoretical methods.[6–16] It has also been extensively studied experimentally by mass spectrometry,[17–19] IR and Raman spectroscopies,[20,21] and photoelectron spectroscopy.[22–26] The

[a]Present address: Yale University, Department of Chemistry, 225 Prospect Street, New Haven, CT 06520-8107.
[b]Present address: Rowland Institute at Harvard, Harvard University, 100 Edwin H. Land Blvd., Cambridge, MA 02142.
[c]Electronic mail: boldyrev@cc.usc.edu
[d]Electronic mail: ls.wan@pnl.gov

vertical detachment energies of Si_6^- have also been computed.[27,28] Of particular interest to the present work was the report by Kishi *et al.*[23] about the photoelectron spectrum of $NaSi_6^-$ at 355 nm, which contained two broad spectral bands approximately at 2.1 and 3.0 eV. Theoretical analysis of the relative stability of several Si_6^{2-} and $NaSi_6^-$ isomers at the MP2/6-31G* and MP4(SDTQ)/6-31G* levels of theory was also carried out by the same authors, who concluded that the most stable structure of $NaSi_6^-$ is based on a C_{2v} Si_6^{2-} fragment, rather than the O_h motif. However, the experimentally determined vertical detachment energy (VDE) (2.10±0.04 eV) and adiabatic detachment energy (ADE) (1.90±0.06 eV) for $NaSi_6^-$ differ significantly from the calculated VDE (1.518 eV) and ADE (1.446 eV) at MP4/6-31G*. Li *et al.*[29] reported that according to their calculations at the B3PW91/6-311G* and MP2(full)/6-311+G* levels of theory, $LiSi_6^-$, $NaSi_6^-$, and KSi_6^- clusters have a $C_{3v}(^1A_1)$ structure for all three species with a cation coordinated to one face of an octahedral Si_6^{2-}. Thus, the global minimum structure of the $NaSi_6^-$ cluster is not yet definitely established.

In the current paper, we present a systematic study of Si_6^{2-} and $NaSi_6^-$ both experimentally and theoretically focusing on elucidating their structures and chemical bonding. Well-resolved photoelectron spectra were obtained for $NaSi_6^-$ at three photon energies (355, 266, and 193 nm), which allow quantitative comparison with the accompanying *ab initio* calculations. The ground state structure of $NaSi_6^-$ was established on the basis of good agreement between the photoelectron spectra and theoretical VDEs, calculated at several levels of theory: CCSD(T)/6-311+G(2*df*), ROVGF/6-311+G(2*df*), and TD-B3LYP/6-311+G(2*df*), all at the B3LYP/6-311+G* geometry. We further investigated the chemical bonding in the most stable isomer of $NaSi_6^-$ and its silicon kernel Si_6^{2-}. Results of MO, natural bond orbital (NBO), and electron localization function (ELF) analyses were compared with those for the octahedral Si_6^{2-} and $B_6H_6^{2-}$ species. We also included photoelectron spectroscopic results on Si_6^- primarily to test theoretical methods used for $NaSi_6^-$.

II. EXPERIMENTAL METHODS

Details of the photoelectron spectroscopy (PES) apparatus have been described elsewhere.[30,31] The silicon cluster anions and Na–Si mixed cluster anions were produced by laser vaporization of a pure Si and a Na/Si mixed target, respectively, in the presence of a helium carrier gas and analyzed by time-of-flight mass spectrometry. The Si_6^- and $NaSi_6^-$ clusters of interests were mass selected and decelerated before being photodetached by a pulsed laser beam, 355 nm (3.496 eV) and 266 nm (4.661 eV) from a Nd:YAG (yttrium aluminum garnet) laser or 193 nm (6.424 eV) from an ArF excimer laser. Photoelectrons were collected at nearly 100% efficiency by a magnetic bottle and analyzed in a 3.5 m long electron flight tube. The PES spectra were calibrated using the known spectra of Au^-, Pt^-, or Cu^-, and the electron energy resolution was $\Delta E_k/E_k \approx 2.5\%$, that is, approximately 25 meV for 1 eV electrons.

III. THEORETICAL METHODS

The search for the global minimum on the potential energy surface of Si_6^{2-} was started with the gradient embedded genetic algorithm (GEGA) program, developed by Alexandrova.[32,33] Semiempirical method PM3 (Refs. 34 and 35) was used for energy, gradient, and force computations, since it provides reasonable quality at low computational costs, which will be important for future studies of large silicon clusters. Our GEGA search produced several low-lying isomers, which were reoptimized at the hybrid B3LYP method[36–38] using the 6-311+G* polarized split-valence basis set,[39–41] at the second order Moller-Plessett (MP2) method,[42–46] and at the coupled-cluster with single, double, and noniterative triple excitations [CCSD(T)] method[47–51] using the 6-311+G* basis set. The total energies of the lowest structures were also estimated at the CCSD(T) level of theory using the extended 6-311+G(2*df*) basis set.

Several levels of theory were used to obtain theoretical VDEs: R(U)CCSD(T)/6-311+G(2*df*), the equation of motion (EOM)-CCSD(T)/6-311+G(2*df*),[52] the restricted and unrestricted outer valence Green function [ROVGF/6-311+G(2*df*) and UOVGF/6-311+G(2*d*)] methods[53–57] (all at the B3LYP/6-311+G* or CCSD(T)/6-311+G* geometries, where available), and the time-dependent (TD) density functional theory[58,59] B3LYP/6-311+G(2*df*) (at the B3LYP/6-311+G* geometries). In the last approach the VDEs were calculated as a sum of the lowest transitions from the ground electronic state of the anion to the lowest electronic state of the neutral species (at the B3LYP level of theory) and the vertical excitation energies in the neutral species (at the TD-B3LYP level of theory) at the anion geometry. At the CCSD(T) and ROVGF levels of theory the electron correlation was treated with frozen core electrons.

Chemical bonding was investigated by means of NBO,[60] ELF,[61–63] and MO analyses. GAUSSIAN 98,[64] GAUSSIAN 03,[65] and MOLPRO 2000.1 (Ref. 66) *ab initio* software packages were used throughout this project. ELF analysis was carried out using the TOPMOD package.[67] MOLEKEL (Ref. 68) and MOLDEN 3.4 (Ref. 69) programs were chosen for the visualization of the ELFs and molecular orbitals, respectively.

IV. EXPERIMENTAL RESULTS

A. Photoelectron spectroscopy of Si_6^-

Figure 1 displays the photoelectron spectra of Si_6^- at three photon energies (355, 266, and 193 nm). Five distinct and intense spectral bands (*X*, *A*, *B*, *C*, and *D*) were observed at 193 nm [Fig. 1(c)] and their VDEs measured from the peak maxima are given in Table I. At 355 nm, the *X* band was better resolved with a well-defined onset, which yielded an ADE of 2.23±0.03 eV and a VDE of 2.35±0.05 eV. Since no vibrational structures were resolved, the ADE, which also represents the electron affinity (EA) of neutral Si_6, was measured by drawing a straight line at the leading edge of the *X* band and then adding the spectral resolution to the intersection with the binding energy axis. The *X* band was quite broad, suggesting significant geometry changes between the ground state of Si_6^- and the corresponding neutral state. Weak and broad signals were observed in between

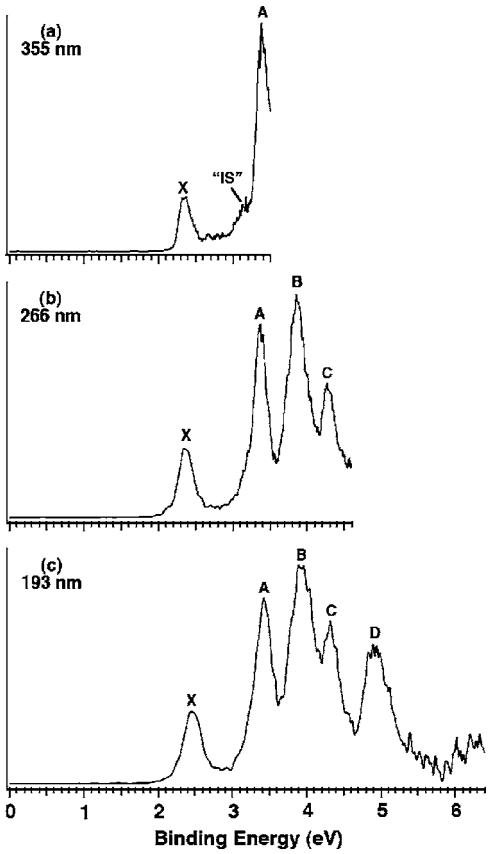

FIG. 1. Photoelectron spectra of Si_6^- at (a) 355 nm (3.496 eV), (b) 266 nm (4.661 eV), and (c) 193 nm (6.424 eV).

bands *X* and *A*, in particular, the feature labeled "IS" was shown as a shoulder on the *A* band. These weak features could be due to either isomers or impurities. Since our mass resolution was high enough to resolve the isotopic pattern of Si_6^-, we could rule out the possibility of impurity contamination. Thus, these features were most likely due to another structural isomer, consistent with previous theoretical calculations.[26,27] The *X-A* band separation defines a highest occupied molecular orbital (HOMO)–lowest unoccupied molecular orbital (LUMO) gap for the neutral Si_6 as 1.05 eV. All the higher energy bands were rather broad, due to either large geometry changes upon photodetachment or overlapping electronic transitions.

The photoelectron spectra of Si_6^- have been reported in a number of previous studies.[22–26] The current study presents a more systematic data set at different photon energies which is in general slightly better than or consistent with those of the previous measurements. The best resolved spectrum for Si_6^- was by Xu *et al.* at 355 nm.[24] Our obtained ADE (2.23 eV) and VDE (2.35 eV) are in good agreement with their corresponding values at 2.22 and 2.36 eV, respectively. However, the shoulder labeled as IS in Fig. 1 was resolved as a vibrational progression by Xu *et al.*, who assigned it as the transition to the first excited state of Si_6. As discussed below, this weak feature is most likely due to the D_{4h} isomer of Si_6^- as shown via the molecular dynamics simulation by Binggeli and Chelikowsky.[27]

B. Photoelectron spectroscopy of $NaSi_6^-$

The photoelectron spectra of $NaSi_6^-$ are shown in Fig. 2 at three photon energies (355, 266, and 193 nm). The electron binding energies of $NaSi_6^-$ are lower than those of Si_6^-, but the overall spectral patterns for the two species are quite similar. Again five distinct and intense spectral bands (*X*, *A*, *B*, *C*, and *D*) were observed for $NaSi_6^-$, which were slightly better spaced than those of Si_6^-. The VDEs of these bands are given in Table II. There appeared two weak features, labeled as *x* and *a*, between bands *X* and *A* in the spectra of $NaSi_6^-$, similar to the weak features observed between the *X* and *A* bands in the spectra of Si_6^-. These two weak features are assigned to be due to a low-lying isomer (Table II), analogous to Si_6^- (*vide infra*). The EA of $NaSi_6$ was measured from the onset of the *X* band of the 355 nm spectrum to be 1.80 ± 0.05 eV, which is 0.43 eV smaller than that of Si_6. The *X-A* band separation of 1.04 eV for $NaSi_6^-$ is identical to that for Si_6^-. In fact, all the five main spectral features of $NaSi_6^-$ line up well with those of Si_6^- with a shift of about 0.4 eV, suggesting that the geometrical and electronic structure of the Si_6 motif in $NaSi_6^-$ is similar to that in Si_6^-.

A very broad and diffuse photoelectron spectrum of $NaSi_6^-$ at 355 nm was reported previously by Kishi *et al.*[23] The current spectra were considerably better resolved, making it possible to quantitatively compare with theoretical calculations (*vide infra*). As shown previously, the combination of PES with *ab initio* calculations is a powerful tool for elucidating the electronic structure and chemical bonding of novel clusters.[70,71] In the following, different levels of theories are employed to assist in the interpretation of the observed photoelectron spectra and to elucidate the detailed structures and the underlying chemical bonding of Si_6^- and $NaSi_6^-$ (Si_6^{2-}).

V. THEORETICAL RESULTS

A. Si_6^-

The two lowest energy structures of Si_6^-, $C_{2v}(^2B_2)$ I and $D_{4h}(^2A_{2u})$ II, (Fig. 3 and Table III) have been identified in the literature.[6–16] According to our calculations the $C_{2v}(^2B_2)$ I and the $D_{4h}(^2A_{2u})$ II structures are almost degenerate. At CCSD(T)/6-311+G(2*df*)//CCSD(T)/6-311+G* level of theory the D_{4h} $(^2A_{2u})$ II structure is slightly more stable (by 0.9 kcal/mol) than the $C_{2v}(^2B_2)$ I structure. We also performed additional calculations for these structures using the CCSD(T) level of theory and three aug-cc-*p*vDZ, aug-cc-*p*vTZ, and aug-cc-*p*vQZ basis sets at the CCSD(T)/6-311+G* geometry. The calculated relative energies for two structures were found to be: 1.41 kcal/mol (DZ), 0.34 kcal/mol (TZ), and 0.13 kcal/mol (QZ) with the D_{4h} $(^2A_{2u})$ structure being more stable. Extrapolation to the infinite basis set showed that the $C_{2v}(^2B_2)$ structure was more stable by 0.02 kcal/mol. Thus, we used both of these structures for our theoretical calculations of VDEs to help interpret the main PES spectral features of Si_6^- (Table I).

TABLE I. Experimental and theoretical vertical detachment energies for Si_6^-. All energies are in eV.

Final configuration		Expt. VDE[a]	TD-B3LYP/6-311+G (2*df*)	UOVGF/6-311+G (2*d*)	EOM/6-311+G (2*df*)	CCSD(*T*)/6-311+G (2*df*)
			$Si_6^-C_{2v}(^2B_2)$			
$^1A_1$ $(4a_1^2 1a_2^2 5a_1^2 3b_2^2 2b_1^2 6a_1^2 4b_2^0)$	*X*	2.35±0.03	2.38	2.17 (0.84)[b]	2.31	2.29
$^3B_2$ $(4a_1^2 1a_2^2 5a_1^2 3b_2^2 2b_1^2 6a_1^1 4b_2^1)$	*A*	3.38±0.03	3.23	3.15 (0.84)[b]	[c]	3.30
$^1B_2$ $(4a_1^2 1a_2^2 5a_1^2 3b_2^2 2b_1^2 6a_1^1 4b_2^1)$	*B*	3.85±0.03	3.65	[d]	3.78	[e]
$^3A_1$ $(4a_1^2 1a_2^2 5a_1^2 3b_2^1 2b_1^2 6a_1^2 4b_2^1)$			3.75	3.61 (0.84)[b]	[c]	3.78
$^3A_2$ $(4a_1^2 1a_2^2 5a_1^2 3b_2^2 2b_1^1 6a_1^2 4b_2^1)$			3.80	3.67 (0.83)[b]	[c]	3.94
$^1A_2$ $(4a_1^2 1a_2^2 5a_1^2 3b_2^2 2b_1^1 6a_1^2 4b_2^1)$			3.96	[d]	4.14	[e]
$^3B_2$ $(4a_1^2 1a_2^2 5a_1^1 3b_2^2 2b_1^2 6a_1^2 4b_2^1)$			4.05	3.93 (0.83)[b]	[c]	[e]
$^1B_2$ $(4a_1^2 1a_2^2 5a_1^1 3b_2^2 2b_1^2 6a_1^2 4b_2^1)$	*C*	4.26±0.03	4.21	[d]	4.44	[e]
$^1A_1$ $(4a_1^2 1a_2^2 5a_1^2 3b_2^1 2b_1^2 6a_1^2 4b_2^1)$			4.23	[d]	4.42	[e]
$^3B_1$ $(4a_1^2 1a_2^1 5a_1^2 3b_2^2 2b_1^2 6a_1^2 4b_2^1)$	*D*	4.89±0.03	4.69	4.61 (0.83)[b]	[c]	4.86
$^3B_2$ $(4a_1^1 1a_2^2 5a_1^2 3b_2^2 2b_1^2 6a_1^2 4b_2^1)$			4.69	4.59 (0.83)[b]	[c]	[e]
$^1B_1$ $(4a_1^2 1a_2^1 5a_1^2 3b_2^2 2b_1^2 6a_1^2 4b_2^1)$			4.92	[d]	5.11	[e]
$^1B_2$ $(4a_1^1 1a_2^2 5a_1^2 3b_2^2 2b_1^2 6a_1^2 4b_2^1)$			5.32	[d]	5.49	[e]
			$Si_6^-D_{4h}(^2A_{2u})$			
$^1A_{1g}$ $(3a_{1g}^2 1e_g^4 1b_{2g}^2 2e_u^4 2a_{2u}^0)$		~2.7[f]	2.74	2.61 (0.92)[b]	[g]	2.63
^3E_g $(3a_{1g}^2 1e_g^4 1b_{2g}^2 2e_u^3 2a_{2u}^1)$		~3.1[f]	3.04	3.05 (0.91)[b]	[g]	3.17
^1E_g $(3a_{1g}^2 1e_g^4 1b_{2g}^2 2e_u^3 2a_{2u}^1)$			3.08	[d]	[g]	[e]
$^3B_{1u}$ $(3a_{1g}^2 1e_g^4 1b_{2g}^1 2e_u^4 2a_{2u}^1)$			4.49	4.53 (0.91)[b]	[g]	4.77
$^3A_{2u}$ $(3a_{1g}^1 1e_g^4 1b_{2g}^2 2e_u^4 2a_{2u}^1)$			4.60	4.63 (0.90)[b]	[g]	4.91
$^1B_{1u}$ $(3a_{1g}^2 1e_g^4 1b_{2g}^1 2e_u^4 2a_{2u}^1)$			4.61	[d]	[g]	[e]
^3E_u $(3a_{1g}^2 1e_g^3 1b_{2g}^2 2e_u^4 2a_{2u}^1)$			4.68	4.71 (0.91)[b]	[g]	4.92
^1E_u $(3a_{1g}^2 1e_g^3 1b_{2g}^2 2e_u^4 2a_{2u}^1)$			5.09	[d]	[g]	[e]
$^1A_{2u}$ $(3a_{1g}^1 1e_g^4 1b_{2g}^2 2e_u^4 2a_{2u}^1)$			5.58	[d]	[g]	[e]

[a]The adiabatic detachment energy or the electron affinity of Si_6 is measured to be 2.23±0.03 eV.
[b]The numbers in the parentheses indicate the pole strength, which characterizes the validity of the one-electron detachment picture.
[c]EOM-CCSD(T) calculations for triplet excited states cannot be performed within our version of the MOLPRO program.
[d]Singlet excited states have two-configurational character and therefore are not reported.
[e]These states cannot be calculated using the CCSD(T) method implemented in Gaussian.
[f]Broad features in Fig. 1(a) between bands *X* and *A*.
[g]These computations were not performed.

B. Si_6^{2-}

For Si_6^{2-} we performed the GEGA search at the semiempirical PM3 level of theory, followed by geometry reoptimization and frequency calculations at higher levels of theory. Two isomers with close energies were obtained: $O_h(^1A_{1g})$ III and $C_{2v}(^1A_1)$ IV (Table IV), as shown in Fig. 3. The octahedral structure consistently remains the global minimum at the B3LYP, MP2, and CCSD(T) levels of the theory (all at 6-311+G* basis set). At our highest level of theory [CCSD(T)/6-311+G(2*df*)//CCSD(T)/6-311+G*] the $O_h(^1A_{1g})$ isomer is 12.2 kcal/mol more stable than the $C_{2v}(^1A_1)$ isomer. The $C_{2v}(^1A_1)$ isomer IV can be considered as a result of a distortion of the $O_h(^1A_{1g})$ isomer III, leading to the cleavage of an "equatorial" Si–Si bond and the formation of a Si–Si bond between the two axial atoms. Alternation of other bond lengths occurs as well, the most noticeable is the increase of the distance between the axial ($Si_{1,2}$) and bridging-equatorial ($Si_{3,4}$) atoms and the decrease of the distance between the axial ($Si_{1,2}$) and the non-bridging-equatorial ($Si_{5,6}$) atoms.

C. $LiSi_6^-$ and $NaSi_6^-$

Due to technical reasons semiempirical GEGA computations could be performed only for the $LiSi_6^-$ system, whose isomers were then taken as starting geometries for higher-level calculations for $NaSi_6^-$. The low-lying $LiSi_6^-$ isomers from the GEGA search contained Si_6^{2-} kernels with both the O_h and C_{2v} structures. Substitution of Li by Na and reoptimization of the obtained structures at the B3LYP/6-311+G* level of theory gave again two low-lying $NaSi_6^-$ isomers (Fig. 3). Geometric parameters as well as harmonic frequencies for structures V and VI are summarized in Table V, where total energies obtained in single-point calculations at CCSD(T)/6-311+G(2*df*) are also given. We found that while for bare Si_6^{2-} the $O_h(^1A_{1g})$ structure III is more stable than the $C_{2v}(^1A_1)$ isomer IV, for $NaSi_6^-$ the $C_{3v}(^1A_1)$ isomer VI with the O_h motif is energetically less favorable than structure V with the C_{2v} motif. At our highest level of theory [CCSD(T)/6-311+G(2*df*)//B3LYP/6-311+G*] the $C_{2v}(^1A_1)$ isomer V of $NaSi_6^-$ is only 1.2 kcal/mol more stable than the $C_{3v}(^1A_1)$ isomer VI. We note that Kishi *et al.* obtained a similar ground state isomer for $NaSi_6^-$.[23] But they did not obtain the C_{3v} isomer; they considered two much higher energy isomers instead, in which the Na^+ is coordinated to either an axial Si atom or to two equatorial Si atoms of O_h Si_6^{2-}.

Comparison of the C_{2v} and O_h structures for the bare Si_6^{2-} with the corresponding fragments in the two $NaSi_6^-$ isomers reveals relatively minor structural changes due to the

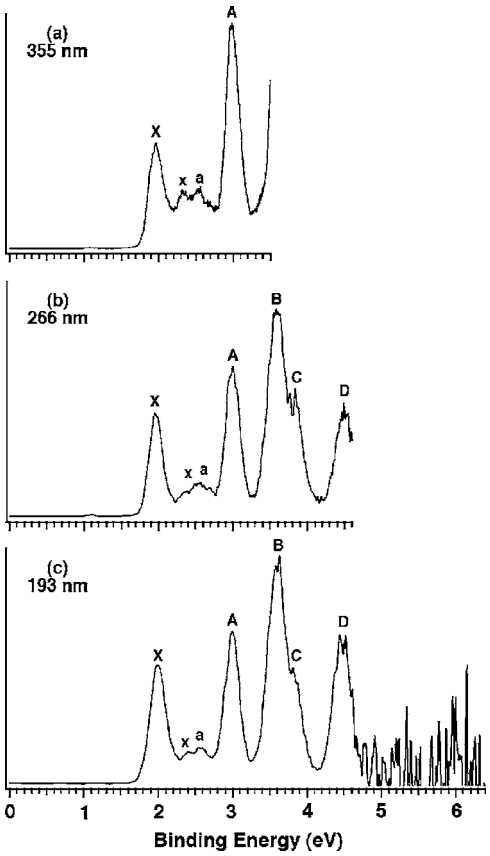

FIG. 2. Photoelectron spectra of $NaSi_6^-$ at (a) 355 nm (3.496 eV), (b) 266 nm (4.661 eV), and (c) 193 nm (6.424 eV).

Na^+ coordination, suggesting the robustness of the silicon kernel as a solid building block. In the global minimum $C_{2v}(^1A_1)$ $NaSi_6^-$, the effect of the Na^+ coordination appears to slightly increase the Si–Si bond length between the two axial atoms (Table V). In the $C_{3v}(^1A_1)$ $NaSi_6^-$ isomer, the Na^+ coordination has little effect on the three proximate Si atoms, but seems to increase the Si–Si bond distances for the three distal Si atoms (Table V).

VI. INTERPRETATION OF THE PHOTOELECTRON SPECTRA

A. Si_6^-

Binggeli and Chelikowsky[27] first computed the PES spectra of Si_6^- using molecular dynamics simulation and compared them with the slightly lower resolution PES spectra reported by Chesnovsky *et al.*[22] They found that the simulated spectrum of the C_{2v} Si_6^- structure was in excellent agreement with the experimental data, whereas a low-lying isomer with a distorted octahedral structure might also make minor contributions to the experimental data. Their study firmly established the C_{2v} ground state structure for Si_6^-. However, a quantitative interpretation of the PES spectra requires detailed calculations for each photodetachment transition from the C_{2v} and D_{4h} ground state structures to the neutral final states. In particular, since the ground state of Si_6^- is a doublet with an unpaired electron, both singlet and triplet final states are possible and they need to be computed in order to make a quantitative comparison with the experimental PES spectra. In the current study, we calculated the VDEs for Si_6^- $(C_{2v}, {}^2B_2)$ at the following levels of theory: CCSD(T)/6-311+G(2*df*)‖CCSD(T)/6-311+G*, EOM/6-311+G(2*df*)‖CCSD(T)/6-311+G*, TD B3LYP/6-311+G(2*df*)‖B3LYP/6-311+G*, and UOVGF/6-311+G(2*d*)‖CCSD(T)/6-311+G*. The final electron configurations and the corresponding detachment energies are given in Table I, compared with the experimental VDEs. The results at the different levels of theory generally agree well with each other and with the experiment.

As shown in Table I, the LUMO of neutral Si_6 is $4b_2$,

TABLE II. Experimental and theoretical vertical detachment energies for $NaSi_6^-$. All energies are in eV.

Feature	VDE (Expt.)	$NaSi_6^-$ $(C_{2v}, {}^1A_1)$ MO	ROVGF/6-311+G (2*df*)[a]	TD-B3LYP/6-311+G (2*df*)[a]	CCSD(T)/6-311+G (2*df*)[a]
X[b]	1.96±0.05	$4b_2$	1.96(0.88)[c]	1.88	1.92
A	3.00±0.05	$6a_1$	2.78(0.89)[c]	2.90	2.94
B	3.60±0.05	$2b_1$	3.46(0.88)[c]	3.32	3.45
		$3b_2$	3.45(0.88)[c]	3.46	[d]
C	3.83±0.05	$5a_1$	3.64(0.88)[c]	3.65	[d]
D	4.50±0.05	$1a_2$	4.42(0.87)[c]	4.26	4.39
		$4a_1$	4.48(0.88)[c]	4.32	[d]
Feature	VDE (Expt.)	$NaSi_6^-$ $(C_{3v}, {}^1A_1)$ MO	ROVGF/6-311+G (2*df*)[a]	TD-B3LYP/6-311+G (2*df*)[a]	
x	2.32±0.03	$5a_1$	2.29(0.88)[c]	2.26	
a	2.55±0.03	$4e$	2.45(0.88)[c]	2.48	
		$3e$	4.30(0.88)[c]	4.32	
		$4a_1$	4.35(0.88)[c]	4.32	

[a]At B3LYP//6-311+G^* geometry.
[b]The adiabatic detachment energy or the electron affinity of $NaSi_6$ is measured to be 1.80±0.05 eV.
[c]The numbers in the parentheses indicate the pole strength, which characterizes the validity of the one-electron detachment picture.
[d]These states cannot be calculated using the CCSD(T) method implemented in Gaussian.

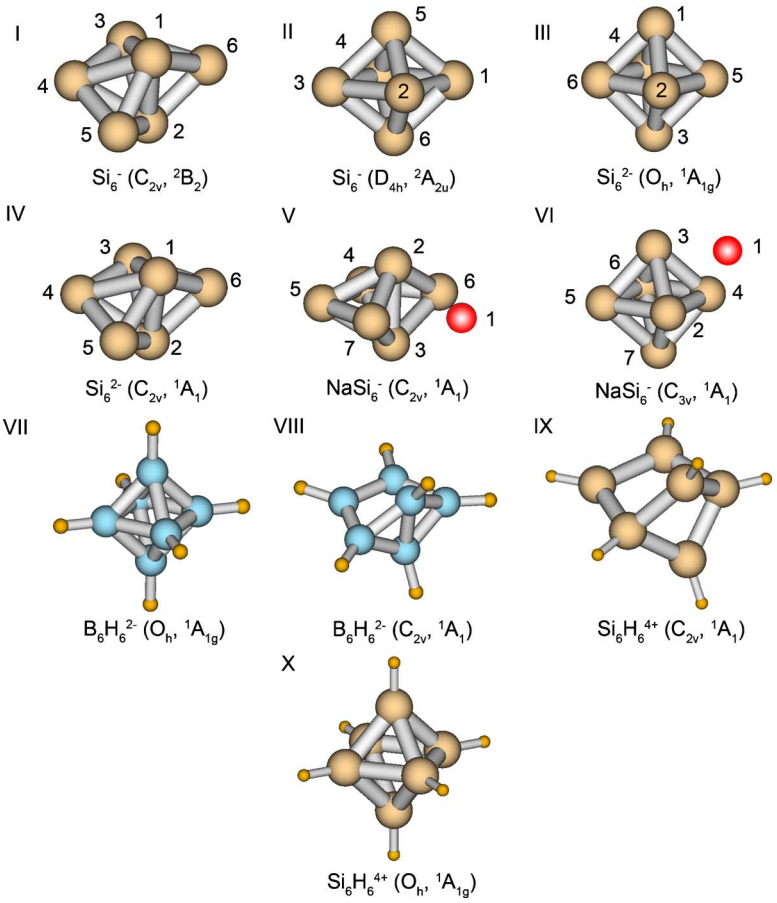

FIG. 3. Structures of isomers for Si_6^- (I, II), Si_6^{2-} (III, IV), $NaSi_6^-$ (V, VI), $B_6H_6^{2-}$ (VII, VIII), and $Si_6H_6^{4+}$ (IX, X).

TABLE III. Calculated molecular properties of $C_{2v}(^2B_2)$ and $D_{4h}(^2A_{2u})$ isomers of Si_6^-.

$C_{2v}(^2B_2)$ method	B3LYP/6-311+G*	MP2/6-311+G*	CCSD(T)/6-311+G*[a,b]	$D_{4h}(^2A_{2u})$ method	B3LYP/6-311+G*	CCSD(T)/6-311+G*[c,d]
$-E$, a.u.	1737.107 496	1734.128 300	1734.184 982	$-E$, a.u.	1737.103 268	1734.179 554
ΔE, kcal/mol	0	0	0	ΔE, kcal/mol	2.7	3.4
$R(Si_1-Si_2)$, Å	2.547	2.525	2.536	$R(Si_1-Si_5)$, Å	2.433	2.414
$R(Si_1-Si_3)$, Å	2.541	2.492	2.527	$R(Si_1-Si_2)$, Å	2.607	2.594
$R(Si_1-Si_6)$, Å	2.402	2.381	2.394	$\omega_1(a_{1g})$, cm^{-1}	313 (0.0)[e]	
$R(Si_3-Si_6)$, Å	2.497	2.471	2.484	$\omega_2(a_{1g})$, cm^{-1}	424 (0.0)[e]	
$R(Si_3-Si_4)$, Å	2.329	2.359	2.328	$\omega_3(a_{2u})$, cm^{-1}	342 (0.2)[e]	
$\omega_1(a_1)$, cm^{-1}	148 (0.1)[e]	163 (0.2)[e]		$\omega_4(b_{1g})$, cm^{-1}	367 (0.0)[e]	
$\omega_2(a_1)$, cm^{-1}	304 (0.2)[e]	332 (0.2)[e]		$\omega_5(b_{2g})$, cm^{-1}	287 (0.0)[e]	
$\omega_3(a_1)$, cm^{-1}	340 (0.0)[e]	355 (0.1)[e]		$\omega_6(b_{2u})$, cm^{-1}	139 (0.0)[e]	
$\omega_4(a_1)$, cm^{-1}	418 (0.5)[e]	427 (0.3)[e]		$\omega_7(e_u)$, cm^{-1}	95 (0.1)[e]	
$\omega_5(a_1)$, cm^{-1}	433 (0.0)[e]	458 (0.7)[e]		$\omega_8(e_u)$, cm^{-1}	391 (10.3)[e]	
$\omega_6(a_2)$, cm^{-1}	110 (0.0)[e]	111 (0.0)[e]		$\omega_9(e_g)$, cm^{-1}	359 (0.0)[e]	
$\omega_7(a_2)$, cm^{-1}	340 (0.0)[e]	406 (0.0)[e]				
$\omega_8(b_1)$, cm^{-1}	207 (3.4)[e]	320 (2.7)[e]				
$\omega_9(b_1)$, cm^{-1}	287 (0.1)[e]	6915[f]				
$\omega_{10}(b_2)$, cm^{-1}	235 (4.0)[e]	255 (1.2)[e]				
$\omega_{11}(b_2)$, cm^{-1}	273 (1.5)[e]	306 (1.7)[e]				
$\omega_{12}(b_2)$, cm^{-1}	436 (4.1)[e]	465 (0.6)[e]				

[a] $E_{tot}=1734.367\ 370$ a.u. at CCSD(T)/6-311+G(2*df*)//CCSD(T)/6-311+G*, $\langle S^2\rangle=0.85$.
[b] $\langle S^2\rangle=0.83$.
[c] $E_{tot}=-1734.368\ 752$ a.u. at CCSD(T)/6-311+G(2*df*)//CCSD(T)/6-311+G*, $\langle S^2\rangle=0.80$.
[d] $\langle S^2\rangle=0.78$
[e] Infrared intensities (km/mol) are given in parentheses.
[f] Symmetry broken problem.

TABLE IV. Calculated molecular properties of $O_h(^1A_{1g})$ and $C_{2v}(^1A_1)$ isomers of Si_6^{2-}.

Method	B3LYP/6-311+G*	MP2/6-311+G*	CCSD(T)/6-311+G*
	Si_6^{2-} $O_h(^1A_{1g})$		
$-E$, a.u.	1737.0441 00	1734.0542 45	1734.112 726[a]
ΔE, kcal/mol	0	0	0
R(Si–Si), Å	2.498	2.464	2.475
$\omega_1(a_{1g})$, cm^{-1}	405 (0.0)[b]	438 (0.0)[b]	431
$\omega_2(e_g)$, cm^{-1}	334 (0.0)[b]	322 (0.0)[b]	332
$\omega_3(t_{1u})$, cm^{-1}	364 (7.4)[b]	379 (9.7)[b]	378
$\omega_4(t_{2g})$, cm^{-1}	333 (0.0)[b]	330 (0.0)[b]	328
$\omega_5(t_{2u})$, cm^{-1}	137 (0.0)[b]	168 (0.0)[b]	146
	Si_6^{2-} $C_{2v}(^1A_1)$		
$-E$, a.u.	1737.031 182	1734.045 549	1734.099 297[c]
ΔE, kcal/mol	8.1	5.5	8.4
$R(Si_1–Si_2)$, Å	2.496	2.461	2.484
$R(Si_1–Si_6)$, Å	2.400	2.384	2.392
$R(Si_1–Si_3)$, Å	2.662	2.595	2.637
$R(Si_3–Si_6)$, Å	2.456	2.453	2.447
$R(Si_3–Si_4)$, Å	2.420	2.407	2.412
$\omega_1(a_1)$, cm^{-1}	158 (4.5)[b]	177 (2.9)[b]	168
$\omega_2(a_1)$, cm^{-1}	287 (4.7)[b]	312 (2.9)[b]	297
$\omega_3(a_1)$, cm^{-1}	343 (2.1)[b]	346 (5.9)[b]	347
$\omega_4(a_1)$, cm^{-1}	355 (0.1)[b]	375 (2.2)[b]	367
$\omega_5(a_1)$, cm^{-1}	419 (2.4)[b]	449 (2.5)[b]	437
$\omega_6(a_2)$, cm^{-1}	129 (0.0)[b]	132 (0.0)[b]	122
$\omega_7(a_2)$, cm^{-1}	332 (0.0)[b]	375 (0.0)[b]	344
$\omega_8(b_1)$, cm^{-1}	151 (6.7)[b]	182 (3.0)[b]	158
$\omega_9(b_1)$, cm^{-1}	236 (0.0)[b]	260 (0.3)[b]	247
$\omega_{10}(b_2)$, cm^{-1}	217 (0.2)[b]	227 (0.1)[b]	221
$\omega_{11}(b_2)$, cm^{-1}	348 (0.2)[b]	345 (0.2)[b]	350
$\omega_{12}(b_2)$, cm^{-1}	436 (3.7)[b]	461 (10.7)[b]	450

[a]E_{tot}=−1734.309 096 a.u. at CCSD(T)/6-311+G(2*df*)//CCSD(T)/6-311+G*.
[b]Infrared intensities (km/mol) are given in parentheses.
[c]E_{tot}=−1734.289 598 a.u. at CCSD(T)/6-311+G(2*df*)//CCSD(T)/6-311+G*.

which is singly occupied in Si_6^-. Detachment of the $4b_2$ electron produces a singlet state ($^1A_1$) for the neutral Si_6. There is a very good agreement between the calculated VDE values among the different theoretical methods (Table I). The next detachment channel involves the $6a_1$ orbital, which is the HOMO of the neutral Si_6. Detachment from this fully occupied MO produces both a triplet and a singlet final state. The calculated VDEs for the triplet final state ($^3B_2$) are in good agreement with the VDE of the *A* band observed experimentally. The *A*-*X* separation, which represents the excitation energy from the ground state of Si_6 ($^1A_1$) to the first excited triplet state ($^3B_2$), is an experimental measure of the HOMO-LUMO gap of neutral Si_6. We note that the TD-B3LYP method underestimates the HOMO-LUMO gap, whereas the CCSD(T) method yields a HOMO-LUMO gap which is in excellent agreement with the experimental measurement.

The next five detachment channels, including the singlet final state ($^1B_2$) obtained by removing the $6a_1$ electron, are congested within a narrow energy range from 3.65 to 4.05 eV from the TD-B3LYP calculations. All these detachment channels contributed to the *B* band, giving rise to the broad PES band. The next two detachment channels ($^1B_2$ and $^1A_1$) are nearly degenerate and their calculated VDEs are in good agreement with that of the *C* band. The next three detachment channels involve removal of an electron from the $1a_2$ orbital and $4a_1$ β orbital. The calculated VDEs to the triplet and singlet states are in the range of the *D* band. The last detachment channel calculated was from the $4a_1$ α orbital with a VDE of 5.32 eV, which could correspond to the tail part of the *D* band, although the signal-to-noise ratio was poor at the high binding energy part.

Overall, the computed VDEs from the C_{2v} Si_6^- are in excellent agreement with the experimental PES spectral pattern, consistent with the previous molecular dynamics simulations by Binggeli and Chelikowsky. These authors were able to obtain simulated spectral patterns very similar to the experimental PES spectra, even though they did not do state-to-state calculations. This was because of the congested nature of the PES spectra and the limited spectral resolution. The current study represents the most quantitative interpretation of the PES spectra of Si_6^-. The spectrum for the low-lying isomer which is a distorted octahedral structure (D_{4h}) was simulated by Binggeli and Chelikowsky. We also obtained theoretical spectra for D_{4h} ($^2A_{2u}$) at the CCSD(T)/6-311+G(2*df*)‖CCSD(T)/6-311+G*, TD-B3LYP/6-311+G(2*df*)‖B3LYP-6-311+G*, and UOVGF/6-311+G(2*d*)‖CCSD(T)/6-311+G* levels of theory (Table I). The theoretical VDE for the ground state transition was

TABLE V. Calculated molecular properties of the $C_{2v}(^1A_1)$ and $C_{3v}(^1A_1)$ isomers of $NaSi_6^-$.

$C_{2v}(^1A_1)$ method	B3LYP/6-311+G*	MP2/6-311+G*	$C_{3v}(^1A_1)$ method	B3LYP/6-311+G*	MP2/6-311+G*
$-E$, a.u.	1899.429 907[a]	1896.020 071	$-E$, a.u.	1899.424 291[b]	1896.009 937
ΔE, kcal/mol	0.0	0.0	ΔE, kcal/mol	3.5	6.4
$R(Na_1-Si_2)$, Å	2.875	2.887	$R(Na_1-Si_2)$	2.861	2.864
$R(Na_1-Si_6)$, Å	2.915	2.913	$R(Na_1-Si_5)$	4.705	4.693
$R(Na_1-Si_4)$, Å	4.578	4.582	$R(Si_2-Si_3)$, Å	2.495	2.471
$R(Si_2-Si_3)$, Å	2.544	2.505	$R(Si_5-Si_6)$, Å	2.548	2.512
$R(Si_2-Si_6)$, Å	2.447	2.428	$R(Si_2-Si_5)$, Å	2.472	2.447
$R(Si_2-Si_4)$, Å	2.553	2.524	$\omega_1(a_1)$, cm^{-1}	213 (7.4)[c]	224 (19.0)[c]
$R(Si_4-Si_6)$, Å	2.443	2.444	$\omega_2(a_1)$, cm^{-1}	328 (5.7)[c]	342 (6.4)[c]
$R(Si_4-Si_5)$, Å	2.504	2.463	$\omega_3(a_1)$, cm^{-1}	359 (31.6)[c]	377 (28.1)[c]
$\omega_1(a_1)$, cm^{-1}	188 (6.9)[c]	203 (5.0)[c]	$\omega_4(a_1)$, cm^{-1}	410 (0.0)[c]	435 (1.7)[c]
$\omega_2(a_1)$, cm^{-1}	230 (19.1)[c]	235 (23.2)[c]	$\omega_5(a_2)$, cm^{-1}	140 (0.0)[c]	186 (0.0)[c]
$\omega_3(a_1)$, cm^{-1}	292 (4.0)[c]	314 (4.2)[c]	$\omega_6(e)$, cm^{-1}	74 (4.2)[c]	92 (4.9)[c]
$\omega_4(a_1)$, cm^{-1}	339 (0.4)[c]	346 (8.1)[c]	$\omega_7(e)$, cm^{-1}	162 (0.0)[c]	197 (0.0)[c]
$\omega_5(a_1)$, cm^{-1}	350 (3.0)[c]	368 (0.2)[c]	$\omega_8(e)$, cm^{-1}	321 (0.3)[c]	316 (0.4)[c]
$\omega_6(a_1)$, cm^{-1}	414 (4.5)[c]	441 (3.2)[c]	$\omega_9(e)$, cm^{-1}	342 (0.0)[c]	360 (0.0)[c]
$\omega_7(a_2)$, cm^{-1}	139 (0.0)[c]	142 (0.0)[c]	$\omega_{10}(e)$, cm^{-1}	375 (9.9)[c]	384 (11.4)[c]
$\omega_8(a_2)$, cm^{-1}	325 (0.0)[c]	360 (0.0)[c]			
$\omega_9(b_1)$, cm^{-1}	90 (2.1)[c]	94 (3.4)[c]			
$\omega_{10}(b_1)$, cm^{-1}	180 (6.2)[c]	204 (2.5)[c]			
$\omega_{11}(b_1)$, cm^{-1}	280 (0.0)[c]	290 (0.5)[c]			
$\omega_{12}(b_2)$, cm^{-1}	143 (3.4)[c]	154 (3.9)[c]			
$\omega_{13}(b_2)$, cm^{-1}	235 (11.6)[c]	247 (8.8)[c]			
$\omega_{14}(b_2)$, cm^{-1}	338 (0.1)[c]	339 (0.1)[c]			
$\omega_{15}(b_2)$, cm^{-1}	414 (1.8)[c]	435 (5.9)[c]			

[a]$E_{tot}=-1896.261\,806$ a.u. at CCSD(T)/6-311+G(2*df*)//B3LYP/6-311+G*.
[b]$E_{tot}=-1896.259\,976$ a.u. at CCSD(T)/6-311+G(2*df*)//B3LYP/6-311+G*.
[c]Infrared intensities (km/mol) are given in parentheses.

~2.61–2.74 eV, consistent with weak signals in the same energy range in Fig. 1. One main feature from this isomer (triplet final state ^3E_g) is in good agreement with the weak feature labeled as IS in Fig. 1, with the rest of the simulated features buried in the features from the C_{2v} ground state of Si_6^-. Our calculations show effective degeneracy of the D_{4h} ($^2A_{2u}$) and C_{2v} ($^2B_2$) isomers; presence of the D_{4h} ($^2A_{2u}$) structure is revealed in all the PES spectra of Si_6^- reported so far, including the current data. The feature labeled IS in Fig. 1 was vibrationally resolved by Xu *et al.*, who did not recognize it as a contribution from a low-lying isomer and attributed it incorrectly to the first excited state transition from the main Si_6^- isomer. Our analysis showed that the theoretical spectrum of Si_6^- C_{2v} ($^2B_2$) was more consistent with the experimental data, demonstrating that under the experimental conditions the C_{2v} structure was more abundant in the molecular beam than the D_{4h} one.

B. $NaSi_6^-$

The ground state of $NaSi_6^-$ can be viewed as adding a Na atom to the C_{2v} ground state of Si_6^-, with an electron transfer from Na to the Si_6 motif to produce the C_{2v} Si_6^{2-} coordinated by a Na^+. The extra electron enters the $4b_2$ singly occupied molecular orbital (SOMO) of Si_6^-, producing a closed shell ground state of $NaSi_6^-$ with a nearly identical MO ordering. The closed shell nature of $NaSi_6^-$ means that the PES spectrum would be simpler because only doublet final states are produced and each occupied MO only yields one detachment channel, in contrast to Si_6^-, where both singlet and triplet final states can be produced after detachment from a fully occupied MO. Table II summarizes the calculated VDEs at several levels of theory for the C_{2v} ground state of $NaSi_6^-$, as well as those for the C_{3v} isomer, compared with the experimental values.

(1) $NaSi_6^-$ (C_{2v}, $^1A_1$). The ground state transition corresponds to an electron detachment from the $4b_2$ HOMO. The ROVGF and CCSD(T) methods yielded VDEs for the ground state transition in exact agreement with the experimental values within the experimental uncertainty (Table II). The second detachment channel is from the $6a_1$ HOMO-1. We note again that the CCSD(T) method yielded a VDE in quantitative agreement with the experimental value of the *A* band. The *X-A* separation measured to be 1.04 eV is also well reproduced by both the TD-B3LYP and CCSD(T) methods. It should be pointed out that the *X-A* separation measured in the spectra of $NaSi_6^-$ is identical to that of Si_6^- (Fig. 1 and Table I), suggesting that the Na^+ coordination has little electronic effect on these MOs. As can be clearly seen from Table II, the next five detachment channels are in excellent agreement with the experimental pattern for the *B*, *C*, and *D* bands, with the *B* and *D* bands each containing two detachment channels. Comparison between the spectra of Si_6^- and $NaSi_6^-$ suggests that the detachment channels of both species are similar. If all the excited singlet states were removed from Si_6^-, one would obtain almost identical spectra for these

two species, which is why the spectra of $NaSi_6^-$ were simpler and less congested. The excellent agreement between the calculated VDEs and the experimental PES data confirms unequivocally that the ground state of $NaSi_6^-$ is the C_{2v} ($^1A_1$) structure V.

(2) $NaSi_6^-$ (C_{3v}, $^1A_1$). The weak features in between the *X* and *A* bands clearly do not belong to the C_{2v} ground state isomer of $NaSi_6^-$. The low-lying C_{3v} ($^1A_1$) isomer VI of $NaSi_6^-$ (Fig. 3) is only 1.2 kcal/mol higher in energy [at CCSD(T)/6-311+G(2*df*)‖B3LYP/6-311+G*] than the global minimum C_{2v} structure and thus could be populated experimentally. As shown in Table II, our calculated VDEs for the first two detachment channels for the C_{3v} isomer are in excellent agreement with the observed weak features (*x* and *a*). The ground state transition from the C_{3v} isomer corresponds to electron detachment from the $5a_1$ HOMO. The computed VDEs from both ROVGF and TD-B3LYP are in very good agreement with the experimental VDE from the *x* feature. The calculated VDE from the 4*e* HOMO-1 gives rise to feature *a*. The two higher binding energy transitions from the C_{3v} isomer have similar binding energies with the *D* band of the main isomer and might be obscured.

Comparisons of the experimental PES data of $NaSi_6^-$ with the theoretical calculations lead to several conclusions. First, two isomers were indeed observed experimentally for $NaSi_6^-$, similarly to Si_6^-. Second, good agreement between the experimental and theoretical VDEs confirms the global minimum (C_{2v}, $^1A_1$) structure V for $NaSi_6^-$ and the low-lying (C_{3v}, $^1A_1$) isomer VI. Third, the Si_6 moiety in $NaSi_6^-$ is very similar electronically and structurally to Si_6^-. Fourth, ROVGF/6-311+G(2*df*), TD B3LYP/6-311+G(2*df*), and CCSD(T)/6-311+G(2*df*) levels of theory, used to calculate VDEs, show good agreement with each other and with experiment. Thus, the first two methods, which do not require as much computer resources as CCSD(T), can be reliably implemented in the future in analyzing PES of larger Na–Si clusters. We note that the poor agreement (>0.5 eV) between the calculated and experimental first VDEs and ADEs of $NaSi_6^-$ reported by Kishi *et al.*[23] was most probably caused by the small basis sets used in their calculations.

VII. CHEMICAL BONDING IN Si_6^{2-} AND $NaSi_6^-$

A. NBO analysis

We performed NBO analysis for the $Si_6^{2-}O_h(^1A_{1g})$, $Si_6^{2-}C_{2v}(^1A_1)$, $NaSi_6^-C_{3v}(^1A_1)$, and $NaSi_6^-C_{2v}(^1A_1)$ species. Tables with the NBO data are available from the authors upon request.

The Si atoms in $Si_6^{2-}O_h(^1A_{1g})$ each carry an effective charge $Q(\mathrm{Si})=-0.333\ |e|$ and their hybridization is $3s^{1.65}3p^{2.62}$. Thus, the $3s^2$ lone pairs on Si show some hybridization with the 3*p* atomic orbitals (AOs) in spite of the excessive −2 charge on the cluster. From $Si_6^{2-}O_h(^1A_{1g})$ to $Si_6^{2-}C_{2v}(^1A_1)$ some charge redistribution occurs. The two axial atoms with $Q(\mathrm{Si}_{1,2})=-0.305\ |e|$ (hybridization $3s^{1.55}3p^{2.70}$) lose some electron density and some *s*-*p* promotion also occurs. The two bridging-equatorial atoms with $Q(\mathrm{Si}_{3,4})=-0.324\ |e|$ (hybridization $3s^{1.66}3p^{2.60}$) are almost the same as in the octahedral structure. The other two non-bridging-equatorial atoms gain some extra negative charge with $Q(\mathrm{Si}_{5,6})=-0.371\ |e|$ and hybridization $3s^{1.67}3p^{2.67}$.

The major difference between the $O_h(^1A_{1g})$ and $C_{2v}(^1A_1)$ structures is the transfer of electron density from lone pairs to Si–Si bonds. The occupation numbers in the six lone pairs in the $O_h(^1A_{1g})$ isomer are 1.965 $|e|$ and 1.964 $|e|$, compared to two lone pairs (Si_1 and Si_2) with occupation numbers 1.703 $|e|$, two lone pairs (Si_3 and Si_4) with occupation numbers 1.914 $|e|$, and two lone pairs (Si_5 and Si_6) with occupation numbers 1.931 $|e|$ in the $C_{2v}(^1A_1)$ isomer. Thus, about 0.5 $|e|$ was transferred from lone pairs in the O_h structure to Si–Si bonds (primarily to Si_3-Si_6 and Si_4-Si_5) in the C_{2v} structure.

NBO analysis of $NaSi_6^-C_{3v}(^1A_1)$ and $C_{2v}(^1A_1)$ revealed that chemical bonding between Na^+ and Si_6^{2-} is highly ionic. The NBO charge for Na is +0.823 $|e|$ in $NaSi_6^-C_{2v}(^1A_1)$ and +0.709 $|e|$ in $NaSi_6^-C_{3v}(^1A_1)$. In both isomers there is some charge redistribution in the corresponding Si_6^{2-} kernels due to the coordination of Na^+. In the C_{2v} structure the axial atoms become more negatively charged [$Q(\mathrm{Si}_{2,3})=-0.419\ |e|$; hybridization $3s^{1.55}3p^{2.82}$], the bridging-equatorial atoms lose some negative charge [$Q(\mathrm{Si}_{4,5})=-0.103\ |e|$; hybridization $3s^{1.69}3p^{2.37}$], and there is almost no change of the charge on the two non-bridging-equatorial atoms [$Q(\mathrm{Si}_{6,7})=-0.391\ |e|$; hybridization $3s^{1.68}3p^{2.68}$]. In the C_{3v} structure, the Si atoms located at the face closest to Na^+ gained some negative charge [$Q(\mathrm{Si}_{2,3,4})=-0.402\ |e|$; hybridization $3s^{1.61}3p^{2.74}$], and the other three atoms become less negatively charged [$Q(\mathrm{Si}_{5,6,7})=-0.168\ |e|$; hybridization $3s^{1.68}3p^{2.44}$].

B. MO analysis

Figure 4 displays the MOs of $Si_6^{2-}C_{2v}$ ($^1A_1$) IV and $NaSi_6^-C_{2v}$ ($^1A_1$) V. Comparison of these two systems shows that the identical sets of orbitals are occupied. From this point of view the chemical bonding in $Si_6^{2-}C_{2v}$ ($^1A_1$) and $NaSi_6^-C_{2v}$ ($^1A_1$) can be assumed to be similar. The same is true for Si_6^{2-} (O_h, $^1A_{1g}$) III and $NaSi_6^-$ (C_{3v}, $^1A_1$) VI.

Upon transition from the O_h ($^1A_{1g}$) isomer of Si_6^{2-} to the C_{2v} ($^1A_1$) isomer a HOMO-LUMO switch occurs, namely, one of the $2t_{1u}$ triply degenerate HOMOs ($3b_1$ in the C_{2v} notation) switches with one of the $1t_{2u}$ triply degenerate LUMOs ($4b_2$ in the C_{2v} notations). One can see from Fig. 5 that the $2t_{1u}$ MO has a significant contribution from the 3*s* AOs of the Si atoms, while the $1t_{2u}$ MO is primarily composed of 3*p* AOs of Si. Thus, the $2t_{1u}$ MO ($3b_1$) to $1t_{2u}$ MO ($4b_2$) switch in the C_{2v} structure should result in decreasing 3*s* AO and increasing 3*p* AO occupations. That is consistent with our observation from the NBO analysis.

One can see from Fig. 4 that the sodium cation can interact more favorably with the $4b_2$ MO rather than with the $3b_1$ MO and that makes the $NaSi_6^-$ (C_{2v}, $^1A_1$) V structure more stable than the $NaSi_6^-$ (C_{3v}, $^1A_1$) VI structure.

Molecular orbitals of $B_6H_6^{2-}O_h$ ($^1A_{1g}$) VII and $Si_6^{2-}O_h$ ($^1A_{1g}$) III are shown in Fig. 5. The sets of the occupied MOs are identical for both systems, but the ordering is slightly different: the HOMO of $B_6H_6^{2-}O_h$ is a triply degenerate $1t_{2g}$ orbital while in Si_6^{2-} it is $2t_{1u}$. Also, $1e_g$ and $2a_{1g}$ orbitals switch their positions.

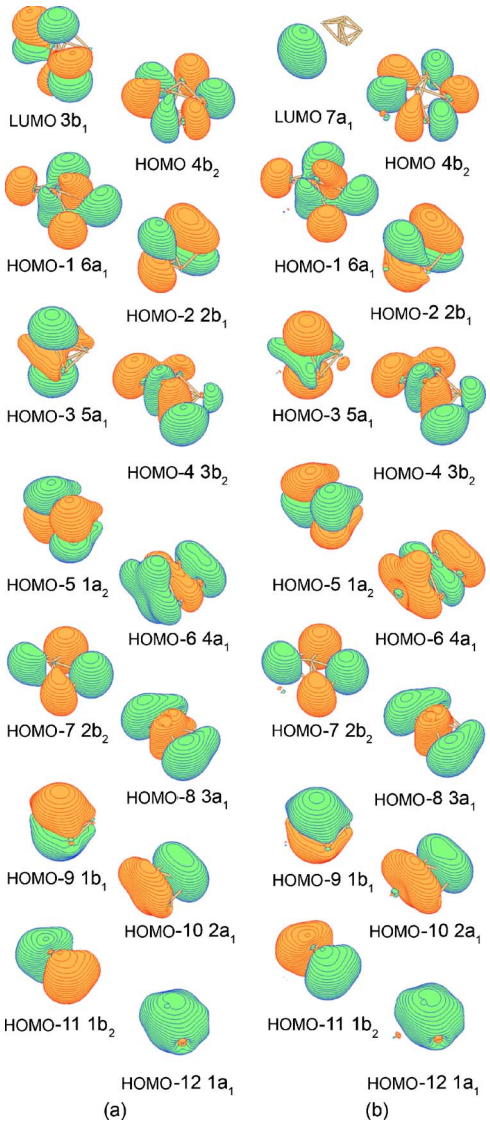

FIG. 4. Molecular orbitals $Si_6^{2-}C_{2v}(^1A_1)$ and $NaSi_6^-C_{2v}(^1A_1)$.

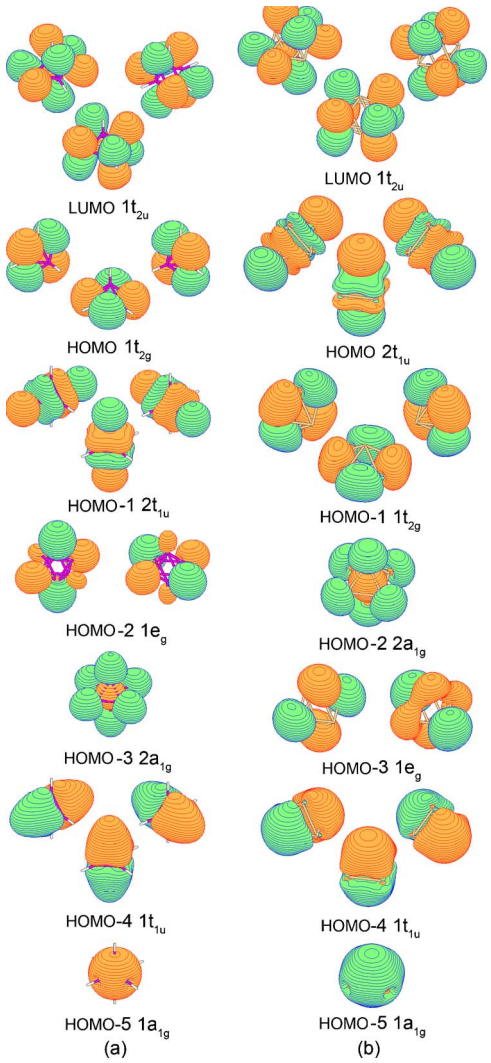

FIG. 5. Molecular orbitals $B_6H_6^{2-}O_h(^1A_{1g})$ and $Si_6^{2-}O_h(^1A_{1g})$.

C. ELF analysis

ELF analysis is a popular modern technique which reveals the regions within a chemical system where pairs of electrons with antiparallel spin can be localized. The local maxima of the ELFs define "localization attractors," of which there are only three basic types: bonding, nonbonding, and core. Bonding attractors lie between the core attractors (which themselves surround the atomic nuclei) and characterize the shared-electron interactions. The spatial organization of localization attractors provides a basis for a well-defined classification of bonds. From any point in space the ELF gradient is followed to an attractor in that region, and this point is then attributed to this attractor. The collection of all the points in space which are assigned to a given attractor is called its basin. The synaptic order of a basin is determined as the number of atomic cores it is connected with. The criterion of discrimination between basins is provided by the reduction of reducible (containing more than one attractor) domains. The reduction of a reducible localization domain occurs at critical values (saddle points) of the bonding isosurface, over which the domain is split into domains containing fewer attractors. The localization domains are then ordered with respect to the ELF critical values, yielding bifurcations.

We studied the ELF of $B_6H_6^{2-}O_h$ $(^1A_{1g})$, $Si_6^{2-}O_h$ $(^1A_{1g})$, $Si_6^{2-}C_{2v}$ $(^1A_1)$, and $NaSi_6^-C_{2v}$ $(^1A_1)$. The ELF bifurcations, leading to the separation of regions with chemical significance, are shown in Fig. 6. Let us start with the comparison of the two octahedral isoelectronic species, $B_6H_6^{2-}O_h$ $(^1A_{1g})$ and $Si_6^{2-}O_h$ $(^1A_{1g})$, which are expected to have similar chemical bonding. The first bifurcation in $B_6H_6^{2-}$ occurs at 0.49 and leads to the separation of six protonated basins (spherelike regions), which correspond to $2e$-$2c$ B–H bonds. There is a similar bifurcation in Si_6^{2-}, but it occurs at a higher ELF value (0.65), and the separated spherelike domains correspond to six lone pairs of the silicon atoms. This means that the interaction of the lone pairs and the skeletal bonds in $O_hSi_6^{2-}$ is stronger than the interaction of the B–H bonds and the skeletal bonds in $O_hB_6H_6^{2-}$. The regions of skeletal bonds are different as well. Bifurcation, separating localization domains in the regions of B–B bonds, occurs at 0.84, revealing 8 domains over the center of each of the octahedron faces and 12 domains connecting these central domains with each other. The bifurcational value is very close to the maximum

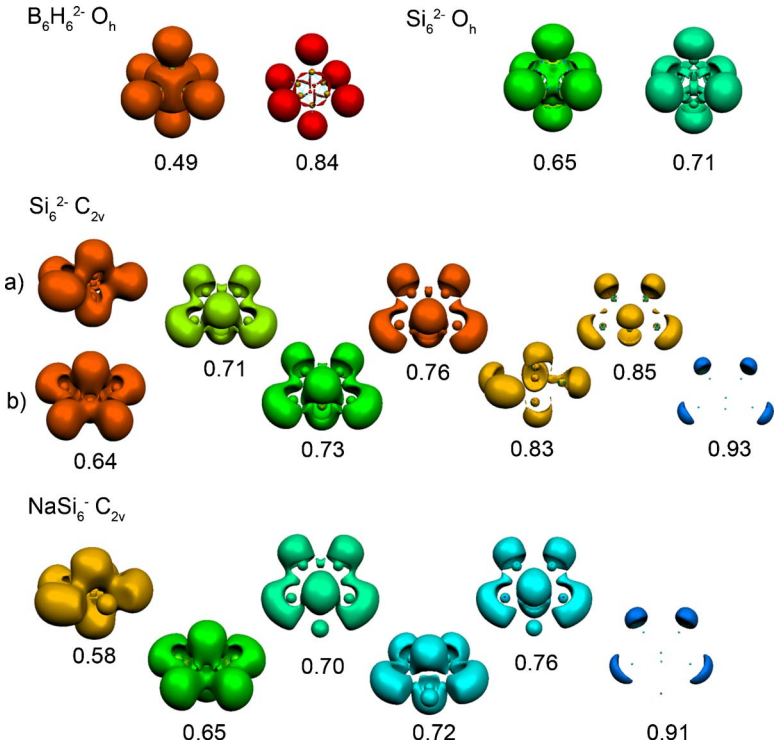

FIG. 6. Bifurcations of ELF for $B_6H_6^{2-}(O_h, {}^1A_{1g})$, $Si_6^{2-}(O_h, {}^1A_{1g})$, $Si_6^{2-}(C_{2v}, {}^1A_1)$, and $NaSi_6^-(C_{2v}, {}^1A_1)$.

value of ELF for these domains (0.85). Thus, there is a very strong interaction between basins of the corresponding attractors, and effectively one six-synaptic basin exists around a single gridlike attractor, covering the entire boron cage. In Si_6^{2-} a similar bifurcation occurs at 0.71 and gives rise to 12 separated localization domains. There are no domains over the centers of the triangular faces of the cluster, the maximum ELF value at the attractors within 12 disynaptic basins, corresponding to the skeletal Si–Si bonds, is 0.78. Thus, the skeletal bonding in $O_hSi_6^{2-}$ is more "localizable" than in $O_hB_6H_6^{2-}$.

In the $C_{2v}Si_6^{2-}$ the first bifurcation occurs at 0.64 and reveals a small bonding domain between the two axial atoms [scheme 0.64(a)], which can be tracked down to the ELF features of σ-antiaromatic $Si_4^0C_{2v}$ $({}^1A_1)$ cluster.[72] At 0.71 bonding domain between bridgelike Si atoms is separated. Bifurcation at 0.73 produces irreducible localization domains, corresponding to the lone pairs of the axial atoms, and the one at 0.76 finally separates lone pairs of the bridge-equatorial atoms. There are two bonding domains in the regions of Si–Si bonding between equatorial atoms, and two more lone pairs, which can be seen after domain reduction at 0.85. So, the interaction between the lone pair domains and the bonding domains is stronger in C_{2v} than in the O_h isomer, which is consistent with our conclusions from the NBO and MO analyses. The last scheme demonstrates that maximal ELF values within the basins corresponding to the axial lone pairs are lower (0.93) than those of equatorial lone pairs (0.98). In other words, the axial lone pairs are less localizable, than the equatorial ones. Scheme 0.64(b) shows ELF saddle points characterizing interaction of the axial lone pairs with the bond between bridge-equatorial atoms. In the $O_hSi_6^{2-}$ isomer ELF maxima (attractors) can be found in the same regions, since irreducible domains exist there. These domains could have disappeared due to the strong interaction with the lone-pair domains as the O_h structure transforms into C_{2v}. The same can be true for bonding domains between the axial and non-bridge-equatorial atoms, since they merge with axial lone pairs at 0.83, but the maximum ELF value for them is between 0.83 and 0.84.

The pattern of chemical bonding in $Si_6^{2-}C_{2v}$ somewhat changes after introduction of Na^+ into the system according to the ELF bifurcational sequence for the $NaSi_6^-C_{2v}$ isomer. The bonding domain between the axial atoms separates at 0.58 (versus 0.64); the bonding domain between bridge-equatorial atoms-separates at 0.70 (versus 0.71). Separation of the axial and two equatorial lone pairs occurs at 0.72 (versus 0.72) and 0.76 (versus 0.76) correspondingly. But there are no bonding domains between bridge and non-bridge-equatorial atoms anymore (which appeared at 0.85 in $Si_6^{2-}C_{2v}$); they merge with lone pair domains of the non-bridge-equatorial atoms. Finally, axial lone pairs have lower maximal ELF values (0.91) than the equatorial ones (0.98).

Chemical bonding analysis of the O_h $({}^1A_{1g})$ isomer of Si_6^{2-} and O_h $({}^1A_{1g})$ isomer of $B_6H_6^{2-}$ revealed that like in our previous study of Si_5^{2-} and $B_5H_5^{2-}$ species,[73] Si_6^{2-} differs from $B_6H_6^{2-}$ by involvement of the electron density, which is supposed to be "lone pairs" of the six silicon atoms in the skeletal bonding in Si_6^{2-}. This tendency of Si atoms in silicon clusters to favor s-p hybridization rather than $3s^2$ lone pairs is also responsible for Si_6^{2-} having two low-lying O_h $({}^1A_{1g})$ and C_{2v} $({}^1A_1)$ isomers. When sodium atom is attached to Si_6^{2-} the alteration in stability occurs. The most stable isomer of $NaSi_6^-$ is based on the Si_6^{2-} kernel with the C_{2v} symmetry. The second most stable isomers of $NaSi_6^-$ is based on the Si_6^{2-} kernel with O_h symmetry.

The two low-lying O_h $({}^1A_{1g})$ and C_{2v} $({}^1A_1)$ isomers of Si_6^{2-} inspired us to test the C_{2v} $({}^1A_1)$ isomer of $B_6H_6^{2-}$. We

found that the C_{2v} ($^1A_1$) isomer VIII of $B_6H_6^{2-}$ (Fig. 3) with the same electronic configuration is not a minimum, but a first order saddle point with the relative energy [compared to the O_h ($^1A_{1g}$) isomer VII] of 65 kcal/mol (at B3LYP/6-311++G**). Thus, even though Si_6^{2-} and $B_6H_6^{2-}$ are valence isoelectronic, they have somewhat different chemical bonding.

D. Protonation as a way to increase the relative stability of the octahedral Si_6^{2-}?

From the above discussion we inferred that in order to stabilize the high symmetry O_h ($^1A_{1g}$) structure of Si_6^{2-} over the C_{2v} ($^1A_1$) structure one has to enforce sp^3 hybridization on Si. In the isoelectronic $B_6H_6^{2-}$ dianion, the external hydrogen atoms enforce almost sp^3 hybridization on boron atoms. We tested if a similar approach will work for silicon by calculating the C_{2v} ($^1A_1$) IX and O_h ($^1A_{1g}$) X structures of $Si_6H_6^{4+}$ at the B3LYP/6-311++G** level of theory (Fig. 3). We checked that both structures have the same electronic configurations as the O_h ($^1A_{1g}$) and C_{2v} ($^1A_1$) structures of Si_6^{2-}. We found that both the C_{2v} ($^1A_1$) IX and O_h ($^1A_{1g}$) X structures of $Si_6H_6^{4+}$ are true local minima at our level of theory, but the C_{2v} ($^1A_1$) IX structure of $Si_6H_6^{4+}$ was found to be significantly more stable (by 19 kcal/mol at B3LYP/6-311++G**) than the O_h ($^1A_{1g}$) X of $Si_6H_6^{4+}$ and that is different from Si_6^{2-} where the O_h ($^1A_{1g}$) III structure is more stable than the C_{2v} ($^1A_1$) IV structure. Thus, protonation is not a solution for stabilization of high symmetric Si_x^{2-} clusters.

VIII. CONCLUSIONS

Well-resolved photoelectron spectra were obtained for Si_6^- and $NaSi_6^-$ at three photon energies (355, 266, and 193 nm) and compared with theoretical calculations to elucidate the structure and bonding in Si_6^- and Si_6^{2-} in $NaSi_6^-$. Global minimum structures of Si_6^{2-} and $NaSi_6^-$ were identified first by using gradient embedded genetic algorithm followed by the B3LYP/6-311+G*, MP2/6-311+G*, and CCSD(T)/6-311+G* (except $NaSi_6^-$) geometry and frequency calculations. By comparing the theoretical VDEs with the experimental data we established the ground state structure for $NaSi_6^-$ to be C_{2v} ($^1A_1$), in which the Na^+ is coordinated to a $C_{2v}Si_6^{2-}$. Though the octahedral Si_6^{2-}, analogous to the closo form of borane $B_6H_6^{2-}$, is the most stable form for the bare dianion, it is not the kernel of the $NaSi_6^-$ global minimum geometry. However, the octahedral Si_6^{2-} coordinated by a Na^+ with C_{3v} ($^1A_1$) symmetry is a low-lying isomer only 1.2 kcal/mol higher in energy and it was observed experimentally.

Chemical bonding analysis of the two low-lying $O_h(^1A_{1g})$ and $C_{2v}(^1A_1)$ isomers of Si_6^{2-} revealed that they differ by switching one of the $2t_{1u}$ triply degenerate HOMOs ($3b_1$ in the C_{2v} notation) with one of the $1t_{2u}$ triply degenerate LUMOs ($4b_2$ in the C_{2v} notations). Because the $2t_{1u}$ triply degenerate HOMO in the $O_h(^1A_{1g})$ isomer contains significant contribution from 3*s* AOs of Si and the $1t_{2u}$ triply degenerate LUMO is composed of primarily 3*p* AOs of Si, such MO exchange resulted in *s*-*p* promotion with increasing *sp* hybridization and increase in Si–Si chemical bonding in the $C_{2v}(^1A_1)$ isomer. When the Na^+ is attached to the Si_6^{2-} cluster in $NaSi_6^-$ it more strongly stabilizes the $4b_2$ MO than the $3b_1$ MO, making the $C_{2v}(^1A_1)$ isomer of $NaSi_6^-$ with the $C_{2v}(^1A_1)Si_6^{2-}$ kernel somewhat more stable than the $C_{3v}(^1A_1)$ isomer of $NaSi_6^-$ with the $O_h(^1A_{1g})Si_6^{2-}$ kernel.

ACKNOWLEDGMENTS

The theoretical work done at Utah was supported by the National Science Foundation (CHE-0404937). The experimental work done at Washington was supported by the National Science Foundation (DMR-0503383) and performed at the W. R. Wiley Environmental Molecular Sciences Laboratory, a national scientific user facility sponsored by DOE's Office of Biological and Environmental Research and located at Pacific Northwest National Laboratory, which is operated for DOE by Battelle. One of the authors (D.Y.Z.) wishes to thank Utah State University for a presidential fellowship. Another author (A.I.B.) wishes to thank the W. R. Wiley Environmental Molecular Science Laboratory and the Chemical Sciences Division, Pacific Northwest National Laboratory for the hospitality and support during this work.

[1] W. N. Lipscomb, *Boron Hydrides* (Benjamin, New York, 1963).
[2] E. L. Muetterties, *Boron Hydride Chemistry* (Academic, New York, 1975).
[3] F. A. Cotton, G. Wilkinson, C. A. Murillo, and M. Bochman, *Advance Inorganic Chemistry*, 6th ed. (Wiley-Interscience, New York, 1999).
[4] J. M. Goicoechea and S. C. Sevov, J. Am. Chem. Soc. **126**, 6860 (2004).
[5] R. B. King, T. Heine, C. Cornminboeuf, and P. v. R. Schleyer, J. Am. Chem. Soc. **126**, 430 (2004).
[6] K. Raghavachari and V. Logovinsky, Phys. Rev. Lett. **55**, 2853 (1985).
[7] G. Pacchioni and J. Koutecky, J. Chem. Phys. **84**, 3301 (1986).
[8] B. P. Feuston, R. K. Kalia, and P. Vashishta, Phys. Rev. B **35**, 6222 (1987).
[9] O. F. Sankey, D. J. Niklewski, D. A. Drabold, and J. D. Dow, Phys. Rev. B **41**, 12750 (1990).
[10] K. Raghavachari and C. M. Rohlfing, J. Chem. Phys. **94**, 3670 (1991).
[11] N. Binggeli, J. L. Martins, and J. R. Chelikowsky, Phys. Rev. Lett. **68**, 2956 (1992).
[12] M. V. Ramakrishna and A. Bahel, J. Chem. Phys. **104**, 9833 (1996).
[13] S. Wei, R. N. Barnett, and U. Landman, Phys. Rev. B **55**, 7935 (1997).
[14] B. X. Li and P. L. Cao, Phys. Rev. B **62**, 15788 (2000).
[15] B. X. Li, P. L. Cao, B. Song, and Z. Z. Ye, Phys. Lett. A **307**, 318 (2003).
[16] C. Majumder and S. K. Kulshreshtha, Phys. Rev. B **69**, 115432 (2004).
[17] L. A. Bloomfield, M. E. Geusic, R. R. Freeman, and W. L. Brown, Chem. Phys. Lett. **121**, 33 (1985).
[18] W. D. Reents and V. E. Bondybey, Chem. Phys. Lett. **125**, 324 (1986).
[19] D. E. Bergeron and A. W. Castleman Jr., J. Chem. Phys. **117**, 3219 (2002).
[20] S. Li, R. J. V. Zee, W. Weltner, Jr., and K. Raghavachari, Chem. Phys. Lett. **243**, 275 (1995).
[21] E. C. Honea, A. Ogura, D. R. Peale, C. Felix, C. A. Murray, K. Raghavachari, W. O. Sprenger, M. F. Jarrold, and W. L. Brown, J. Chem. Phys. **110**, 12161 (1999).
[22] O. Chesnovsky, S. H. Yang, C. L. Pettiette, M. J. Craycraft, Y. Liu, and R. E. Smalley, Chem. Phys. Lett. **138**, 119 (1987).
[23] R. Kishi, H. Kawamata, Y. Negishi, S. Iwata, A. Nakajima, and K. Kaya, J. Chem. Phys. **107**, 10029 (1997).
[24] C. Xu, T. R. Taylor, G. R. Burton, and D. M. Neumark, J. Chem. Phys. **108**, 1395 (1998).
[25] M. A. Hoffmann, G. Wrigge, B. V. Issendorff, J. Muller, G. Gantefor, and H. Haberland, Eur. Phys. J. D **16**, 9 (2001).
[26] L. Kronik, R. Fromherz, E. Ko, G. Gantefor, and J. R. Chelikowsky, Eur. Phys. J. D **24**, 33 (2003).
[27] N. Binggeli and J. R. Chelikowsky, Phys. Rev. Lett. **75**, 493 (1995).
[28] C. Zhao and K. Balasubramanian, J. Chem. Phys. **116**, 3690 (2002).
[29] S.-D. Li, G.-M. Ren, and Z.-H. Jin, J. Chem. Phys. **119**, 10063 (2003).

[30] L. S. Wang, H. S. Cheng, and J. Fan, J. Chem. Phys. **102**, 9480 (1995).
[31] L. S. Wang and H. Wu, in *Cluster Materials*, Advances in Metal and Semiconductor Clusters Vol. IV, edited by M. A. Duncan (JAI, Greenwich, 1998), p. 299.
[32] A. N. Alexandrova, A. I. Boldyrev, Y.-J. Fu, X.-B. Wang, and L.-S. Wang, J. Chem. Phys. **121**, 5709 (2004).
[33] A. N. Alexandrova and A. I. Boldyrev, J. Chem. Theory Comput. **1**, 566 (2005).
[34] J. J. P. Stewart, J. Comput. Chem. **10**, 209 (1989).
[35] J. J. P. Stewart, J. Comput. Chem. **10**, 221 (1989).
[36] R. G. Parr and W. Yang, *Density-Functional Theory of Atoms and Molecules* (Oxford University Press, Oxford, 1989).
[37] A. D. Becke, J. Chem. Phys. **98**, 5648 (1993).
[38] J. P. Perdew, J. A. Chevary, S. H. Vosko, K. A. Jackson, M. R. Pederson, D. J. Singh, and C. Fiolhais, Phys. Rev. B **46**, 6671 (1992).
[39] R. Krishnan, J. S. Binkley, R. Seeger, and J. A. Pople, J. Chem. Phys. **72**, 650 (1980).
[40] A. D. McLean and G. S. Chandler, J. Chem. Phys. **72**, 5639 (1980).
[41] T. Clark, J. Chandrasekhar, G. W. Spitznagel, and P. v. R. Schleyer, J. Comput. Phys. **4**, 294 (1983).
[42] M. Head-Gordon, J. A. Pople, and M. J. Frisch, Chem. Phys. Lett. **153**, 503 (1988).
[43] M. J. Frisch, M. Head-Gordon, and J. A. Pople, Chem. Phys. Lett. **166**, 275 (1990).
[44] M. J. Frisch, M. Head-Gordon, and J. A. Pople, Chem. Phys. Lett. **166**, 281 (1990).
[45] M. Head-Gordon and T. Head-Gordon, Chem. Phys. Lett. **220**, 122 (1994).
[46] S. Saebo and J. Almlof, Chem. Phys. Lett. **154**, 83 (1989).
[47] J. Cizek, Adv. Chem. Phys. **14**, 35 (1969).
[48] G. D. Purvis and R. J. Bartlett, J. Chem. Phys. **76**, 1910 (1982).
[49] G. E. Scuseria, C. L. Janssen, and H. F. Schaefer III, J. Chem. Phys. **89**, 7382 (1988).
[50] G. E. Scuseria and H. F. Schaefer III, J. Chem. Phys. **90**, 3700 (1989).
[51] J. A. Pople, M. Head-Gordon, and K. Raghavachari, J. Chem. Phys. **87**, 5968 (1987).
[52] C. Hampel, K. Peterson, and H.-J. Werner, Chem. Phys. Lett. **190**, 1 (1992).
[53] L. S. Cederbaum, J. Phys. B **8**, 290 (1975).
[54] V. G. Zakrzewski and J. V. Ortiz, Int. J. Quantum Chem. **53**, 583 (1995).
[55] J. V. Ortiz, Int. J. Quantum Chem., Quantum Chem. Symp. **23**, 321 (1989).
[56] For a review see J. V. Ortiz, V. G. Zakrzewski, and O. Dolgunitcheva, Conceptual Perspective in Quantum Chemistry **3**, 465 (1997), edited by Y.-L. Calais and E. Kryackko (Kluver, Dordrecht, 1997).
[57] Yu. Dahnovsky, V. G. Zakrzewski, A. Klesov, and J. V. Ortiz, J. Chem. Phys. **123**, 184711 (2005).
[58] R. Bauernshmitt and R. Alrichs, Chem. Phys. Lett. **256**, 454 (1996).
[59] M. E. Casida, C. Jamorski, K. C. Casida, and D. R. Salahub, J. Chem. Phys. **108**, 4439 (1998).
[60] F. Weinhold and C. Landis, *Valency and Bonding. A Natural Bond Orbital Donor-Acceptor Perspective* (Cambridge University Press, Cambridge, UK, 2005).
[61] A. D. Becke and K. E. Edgecombe, J. Chem. Phys. **92**, 5397 (1990).
[62] A. Savin, B. Silvi, and F. Colonna, Can. J. Phys. **74**, 1088 (1996).
[63] A. Savin, R. Nesper, S. Wengert, and T. F. Fassler, Angew. Chem., Int. Ed. Engl. **36**, 1808 (1997).
[64] M. J. Frisch, G. M. Trucks, H. B. Schlegel *et al.*, GAUSSIAN 98, Revision A.7, Gaussian, Inc., Pittsburgh, PA, 1998.
[65] M. J. Frisch, G. M. Trucks, H. B. Schlegel *et al.*, GAUSSIAN 03, Revision A.1, Gaussian, Inc., Pittsburgh, PA, 2003.
[66] H.-J. Werner, P. J. Knowles, R. D. Amos *et al.*, MOLPRO-2000.1.
[67] S. Noury, X. Krokidis, F. Fuster, and B. Silvi, TOPMOD Package, Universite Pierre et Marie Curie, 1997; Comput. Chem. (Oxford) **23**, 597 (1999).
[68] S. Portmann, MOLEKEL, Version 4.3., CSCS/ETHZ, 2002.
[69] G. Schaftenaar, MOLDEN 3.4, CAOS/CAMM Center, The Netherlands, 1998.
[70] A. I. Boldyrev and L. S. Wang, J. Phys. Chem. A **105**, 10759 (2001).
[71] A. I. Boldyrev and L. S. Wang, Chem. Rev. (Washington, D.C.) **105**, 3716 (2005).
[72] H.-J. Zhai, A. E. Kuznetsov, A. I. Boldyrev, and L. S. Wang, ChemPhysChem **5**, 1885 (2004).
[73] D. Yu. Zubarev, A. I. Boldyrev, X. Li, L.-F. Cui, and L. S. Wang, J. Phys. Chem. A **109**, 11385 (2005).